Molecular Imaging of Tumor Microenvironment to Assess the Effects of Locoregional Treatment for Hepatocellular Carcinoma

Quan Chen [ID],[1,2] Austin Z. Chen,[1] Guorong Jia,[1] Jindian Li,[1] Chuansheng Zheng [ID],[2] and Kai Chen [ID] [1]

Liver cancer is one of the leading causes of cancer deaths worldwide. Among all primary liver cancers, hepatocellular carcinoma (HCC) is the most common type, representing 75%-85% of all primary liver cancer cases. Median survival following diagnosis of HCC is approximately 6 to 20 months due to late diagnosis in its course and few effective treatment options. Interventional therapy with minimal invasiveness is recognized as a promising treatment for HCC. However, due to the heterogeneity of HCC and the complexity of the tumor microenvironment, the long-term efficacy of treatment for HCC remains a challenge in the clinic. Tumor microenvironment, including factors such as hypoxia, angiogenesis, low extracellular pH, interstitial fluid pressure, aerobic glycolysis, and various immune responses, has emerged as a key contributor to tumor residual and progression after locoregional treatment for HCC. New approaches to noninvasively assess the treatment response and assist in the clinical decision-making process are therefore urgently needed. Molecular imaging tools enabling such an assessment may significantly advance clinical practice by allowing real-time optimization of treatment protocols for the individual patient. This review discusses recent advances in the application of molecular imaging technologies for noninvasively assessing changes occurring in the microenvironment of HCC after locoregional treatment. (*Hepatology Communications* 2022;6:652-664).

Hepatocellular carcinoma (HCC) is one of the leading causes of cancer deaths worldwide.[1,2] Although surgical extirpation and transplantation are the curative treatment for early-stage patients, locoregional treatment (LRT) is playing an increasing role in the management of HCC.[3] LRT for HCC includes (1) intra-arterial therapy (IAT), which consists of transarterial chemoembolization (TACE), conventional TACE, drug-eluting beads TACE, transarterial radioembolization, and selective internal radiation therapy; and (2) ablation, including radiofrequency ablation (RFA), microwave ablation (MWA), and percutaneous ethanol injection (PEI)[4,5] (Fig. 1). LRT is recommended for patients with HCC at different stages guided by the Barcelona Clinic Liver Cancer (BCLC) staging system, such as the very early

(BCLC stage 0), early (BCLC stage A), intermediate stages (BCLC stage B), and even advanced stage (BCLC stage C).[3-5] However, increasing evidence indicates that changes in the tumor microenvironment (TME) of HCC after LRT may stimulate tumor proliferation, angiogenesis, treatment resistance, tumor recurrence, and metastasis, which limit the long-term efficacy of LRT.[6-11] Therefore, effectively monitoring the changes of TME in real time is particularly important for optimizing the strategy of LRT for HCC.

Although a few invasive approaches, such as oxygen electrodes[8] and microvessel density (MVD),[12] are available to monitor TME in HCC, most invasive methods may induce or accelerate tumor metastasis. Thus, the noninvasive methods that can be used to access the changes of TME in HCC are favorable and of great significance. Molecular imaging as an emerging technology enables the noninvasive visualization, characterization, and quantification of molecular events in living subjects.[13-15] The commonly used molecular imaging modalities include (1) positron emission tomography (PET) and single-photon emission computed tomography (SPECT); (2) magnetic resonance imaging (MRI); (3) optical imaging (OI), such as bioluminescence imaging and fluorescence imaging (FLI); and (4) contrast-enhanced ultrasound (US) and photoacoustic imaging (PAI) (Table 1). With the development of molecular imaging techniques, hybrid imaging modalities, such as PET/CT and PET/MRI, are proving to be invaluable, as they can provide comprehensive anatomic and functional information by taking the strengths of modalities.

In this review, we summarize the recent applications of molecular imaging to assess the TME in HCC post-locoregional therapy. Comments and future perspectives on the development of imaging techniques in this field are also provided.

Characterization of TME After LRT in HCC

The TME of HCC is a highly heterogeneous ecosystem composed of noncellular and cellular components, and it plays a key role in regulating liver fibrosis, liver cancer, epithelial–mesenchymal transition (EMT), tumor invasion, and metastasis.[6,16] The noncellular components of tumor stroma are usually characterized by extracellular matrix proteins, proteolytic enzymes, growth factors, and inflammatory cytokines, regulating HCC biology by influencing tumor signaling pathways in tumor cells. The cellular components consist primarily of, for example, HCC cells, HCC-related fibroblasts, immune cells, and endothelial cells. The interaction between tumor and stroma plays an active role in the recruitment and metabolic reprogramming of stromal cells in TME.[17-20]

Changes in the TME after LRT of HCC are often characterized by hypoxia, tumor angiogenesis,

ARTICLE INFORMATION:

From the [1]Department of Radiology, Keck School of Medicine, University of Southern California, Los Angeles, CA, USA; [2]Department of Radiology, Union Hospital, Tongji Medical College, Huazhong University of Science and Technology, Wuhan, China.

ADDRESS CORRESPONDENCE AND REPRINT REQUESTS TO:

Kai Chen, Ph.D.
Department of Radiology
Keck School of Medicine
University of Southern California, Los Angeles
Los Angeles, California, USA
E-mail: chenkai@med.usc.edu
Tel.: +1-323-442-3582

Chuansheng Zheng, M.D., Ph.D.
Department of Radiology
Union Hospital
Tongji Medical College
Huazhong University of Science and Technology
Wuhan, China
E-mail: hqzcsxh@sina.com
Tel.: +86-027-85353238
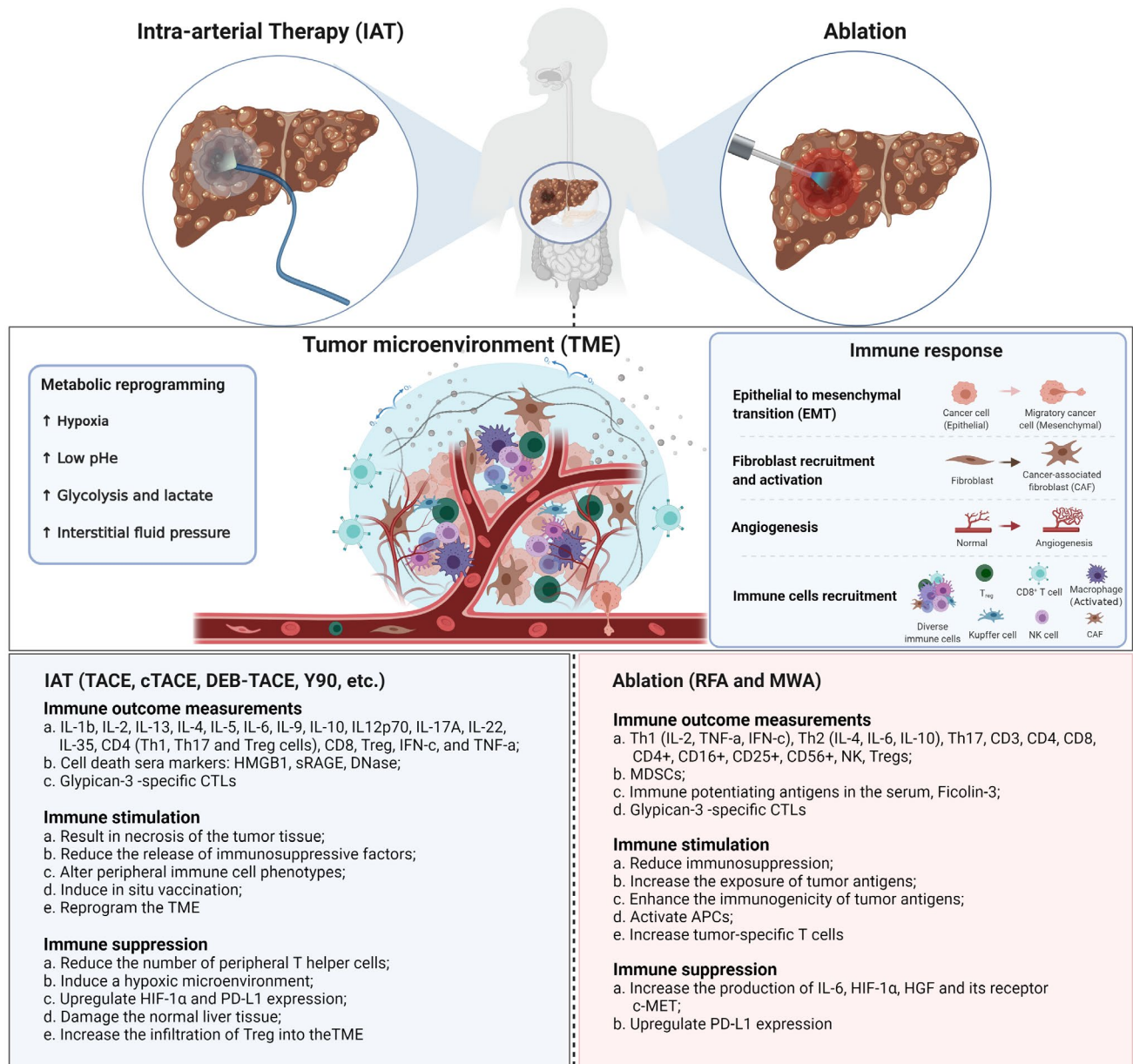
FIG. 1. The landscape of immunosuppressive TME of HCC after LRT, including metabolic reprogramming and various immune responses, such as immune stimulation, immune suppression, and immune evasion. Changes in the TME after LRT of HCC are often characterized by hypoxia low extracellular pH, up-regulation of glycolysis, increased interstitial fluid pressure, and tumor angiogenesis. Various immune outcomes can be measured after intra-arterial therapy and tumor ablation.

up-regulation of glycolysis, low extracellular pH (pHe), increased interstitial fluid pressure, and various immune response, such as immune stimulation, immune suppression, and immune evasion, which is usually associated with tumor residue, recurrence, metastasis, and treatment resistance.[11,21,22] TACE and RFA can expose residual cancer cells to a hypoxic

TME.[7,10] Detrimental effects of hypoxia in carcinogenesis include (1) induction of a more aggressive tumor phenotype (up-regulation of growth factors, induction of apoptosis resistance, DNA hypermethylation of tumor suppressor genes, and induction of EMT); (2) increased expression of immune checkpoints and impaired antitumor immune response, such

TABLE 1. MAJOR MOLECULAR IMAGING MODALITIES

Imaging Modality	Detection	Spatial Resolution	Temporal Resolution	Advantages	Disadvantages	Application
PET	γ-ray	1-2 mm (microPET); 6-10 mm (clinical PET)	Second to minutes	High sensitivity; quantitative whole-body scanning; no tissue penetrating limit	Radiation risk; high cost; low spatial resolution	Functional imaging
SPECT	γ-ray	0.5-2 mm (microSPECT); 7-15 mm (clinical SPECT)	Minutes	High sensitivity; no tissue penetrating limit	Radiation risk; low spatial resolution	Functional imaging
MRI	Magnetic field	0.01-0.1 mm (small-animal MRI); 0.5-1.5 mm (clinical MRI)	Minutes to hours	High spatial resolution; no tissue penetrating limit; no radiation risk	Relatively low sensitivity; long imaging time; exogenous contrast agent; low edge contrast	Anatomical/functional imaging
Fluorescence imaging	Fluorescence	2-3 mm	Second to minutes	High sensitivity; multiplexed imaging	Low spatial resolution; poor tissue penetration; high degree of scattering	Functional imaging
Bioluminescence imaging	Fluorescence	3-5 mm	Second to minutes	High sensitivity; high throughput	Relying on luciferin; requiring excitation (external light source); low potential for clinical translation	Functional imaging
US	Ultrasonic waves	0.01-0.1 mm for superficial (few mm depth) applications; 1-2 mm for deeper (few cm depths) applications	Second to minutes	Real time; low cost; portable	Low resolution; operator-dependent analysis	Anatomical/functional imaging
PAI	Ultrasonic waves	~0.01 to 1 mm	Second to minutes	Higher resolution (from optical tomography); deeper penetration (from ultrasonography); high optical contrast; low acoustic scattering	Shielding by strongly absorbing objects	Anatomical/functional imaging

TABLE 2. IMAGING MODALITIES USED FOR THE ASSESSMENT OF TME IN HCC

TME	Imaging Modalities	Biological Targets	Imaging Probes and Methods	Preclinical and/or Clinical Studies	References
Hypoxia	PET/CT	NTR	^{18}F-FMISO, ^{124}I- IAZGP, ^{18}F-EF1, ^{18}F-EF5	Preclinical and clinical	[24-27]
		pO$_2$	^{18}F-FDG, perfusion CT	Preclinical	[86]
	MR	Oxygen-sensitive	BOLD, TOLD	Preclinical and clinical	[28,29]
		HIF-1α	DW-MRI, DCE-MRI	Preclinical and clinical	[30,31]
	OI	NTR	BBP	Preclinical	[32]
	PAI	HIF-1α	sO$_2$	Preclinical	[33]
Angiogenesis	PET/SPECT	Integrin $\alpha_v\beta_3$	^{64}Cu-cyclam-RAFT-c(-RGDfK-)4, ^{99m}Tc-3PRGD2	Preclinical	[34,35]
	SPECT	CD13	^{99m}Tc-NGR	Preclinical	[36]
	MR	Angiogenesis	DCE-MRI, DW-MRI, ASL-MRI, BOLD-MRI	Preclinical and clinical	[37-40]
		Integrin $\alpha_v\beta_3$	RGD-modified T1-Fe$_3$O$_4$	Preclinical	[41]
		VEGFR	IONP	Preclinical	[42]
	US	Integrin $\alpha_v\beta_3$, VEGFR	Microbubbles	Preclinical	[43,44]
		Angiogenesis	CEUS, 3D DCE-US	Preclinical	[45,46]
Low pHe	SPECT/PAI	pH-sensitive	^{131}I-Pd-PEG or ^{125}I-Pd-PEG	Preclinical	[47]
	MR	pH-sensitive	^{31}P MRSI, HP ^{13}C MRSI, CEST, pHe mapping, IONP	Preclinical	[48-50]
	OI	pH-sensitive	pH-sensitive nanoprobes	Preclinical	[51]
Glycolysis and lactate	PET	Metabolic parameters	^{18}F-FDG	Preclinical and clinical	[22,52-54]
	MR	PKM2	Hyperpolarized ^{13}C-MRSI, ^{13}C-Pyruvate	Preclinical	[53,55]
IFP	CT	Liposomes	DCE-CT	Preclinical	[56,87]
	MR	IFP	DCE-MRI	Preclinical	[57]
Immune cells	MR	CD3+ and CD8+ T cells	Radiomics (Immunoscore and Rad score)	Preclinical and clinical	[61,62]
		Macrophages	SPIONs	Preclinical	[68]
	OI	TILs	IRDye800-AbOX40	Preclinical	[60]
CAFs	PET	FAPI	^{68}Ga-FAPI	Preclinical and clinical	[63,64]
MMPs	MR/OI	MMP-2	Gd–Au@IR820	Preclinical	[65]
	OI	MMP	NIR dye	Preclinical	[66]
APCs	MR	HLA-DR antibodies	^{160}Gd-HLA-DR antibodies	Preclinical	[68]
GPC3	PET	GPC3	^{89}Zr-αGPC3, Al[^{18}F]F-GP2633	Preclinical	[70,73]
	OI	GPC3	GSI-Lip, Cy5.5-GBP	Preclinical	[71,72]

Abbreviations: BBP, *n*-butyl benzyl phthalate; CEST, chemical exchange saturation transfer; HLA, human leukocyte antigen IONP, iron oxide nanoparticle; SPION, superparamagnetic iron oxide nanoparticle; TOLD, tissue oxygen level–dependent.

as impaired entry of antitumor immune cells, recruitment of immunosuppressive regulatory T cells (Tregs), and myeloid-derived suppressor cells (MDSCs); (3) stimulation of angiogenesis; (4) up-regulation of glycolysis; (5) low pHe; and (6) increased interstitial fluid pressure (IFP).[7] In addition, changes in the immune response are often observed in patients with HCC after LRT.[9] LRT, including but not limited to TACE, MWA, RFA and Yttrium-90 (Y90), can cause various immune responses[9,23] (Fig. 1). It is worthwhile to mention that the TME change could be treatment-specific. For example, the main therapeutic effect of TACE is via ischemic tumor necrosis due to the embolic effect, while local ablation provides treatment via thermal damage to cancer. In addition, Y90 has no embolic or thermal effect but radiation can induce tumor necrosis with slower therapeutic effect than TACE or ablation. Various molecular imaging techniques are being developed for accessing the changes of TME in HCC (Table 2).

Molecular Imaging of TME After LRT in HCC

HYPOXIA

Hypoxia can be assessed by hypoxia markers using molecular imaging modalities, such as PET,

MRI, OI, and PAI. Nitroreductase (NTR), hypoxia-inducible factor 1 alpha (HIF-1α), and carbonic anhydrase IX (CA-IX) are the major targets used for noninvasive imaging of tumor hypoxia. A variety of NTR-targeted radionuclide-labeled imaging agents, such as ^{18}F-FMISO,[24] ^{124}I-IAZG,[24,25] ^{18}F-EF1[26] and ^{18}F-EF5,[27] have been developed for detecting the hypoxia region of HCC using PET imaging. The development of new oxygen-sensitive MRI techniques makes it possible to noninvasively detect the perfusion and oxygenation state of tumors.[8,17,28,29] For example, blood oxygen level–dependent (BOLD) and tissue oxygen level–dependent MRI have been used in preclinical and clinical studies to assess the blood supply and oxygenation of HCC.[28,29] The apparent diffusion coefficient in diffusion-weighted MRI (DW-MRI) and volume transfer constant (Ktrans), area under the curve (AUC) in dynamic contrast-enhanced MRI (DCE-MRI) are related to hypoxia markers, such as HIF-1α, CA-IX, and vascular endothelial growth factor (VEGF). Therefore, DW-MRI and DCE-MRI have been used to assess cell proliferation and hypoxia in HCC.[30,31] In addition, NTR-targeted fluorescent probes, such as *n*-butyl benzyl phthalate,[32] have shown the potential of detecting hypoxia of HCC by OI. A recent study demonstrated that PAI is useful for noninvasive monitoring of the changes of tissue oxygen saturation in a rodent model of HCC treated with sorafenib.[33]

ANGIOGENESIS

Several targets of tumor angiogenesis, such as integrin $\alpha_v\beta_3$ and VEGF, are being intensively investigated to evaluate tumor angiogenesis in HCC by molecular imaging. For instance, the radiolabeled tracers, ^{64}Cu-cyclam-RAFT-c(-RGDfK-)4[34] and ^{99m}Tc-3PRGD2,[35] were studied for monitoring integrin $\alpha_v\beta_3$ by PET and SPECT, whereas ^{99m}Tc-NGR[36] was prepared for targeting CD13 by SPECT. The vascular MRI techniques can be generally divided into two groups: (1) direct detection of angiogenesis with extrinsic contrast agents, such as DCE-MRI and MRI with targeted agents; and (2) indirect detection of angiogenesis without contrast agents, such as arterial spin labeling (ASL) and BOLD-MRI.[37] DCE-MRI was used to measure the enhancement of exogenous contrast. On the other hand, ASL-MRI, BOLD-MRI, and DW-MRI have been used to measure the enhancement of endogenous contrast.[37-39] The quantitative parameter Ktrans and semi-quantitative parameter iAUC60 of DCE-MRI are related to MVD, which can noninvasively assess tumor angiogenesis in the VX2 liver tumor model after PEI.[40] Additionally, the Arg-Gly-Asp (RGD)-modified T1-Fe$_3$O$_4$ was used as a highly sensitive positive contrast agent targeting integrin $\alpha_v\beta_3$, and it can monitor angiogenesis of HCC by MRI.[41] Iron oxide nanoparticles also showed the utility of detecting the local sorafenib delivery to HCC for targeted embolotherapy and visualizing the distribution of microspheres using MRI.[42] Furthermore, integrins $\alpha_v\beta_3$ and VEGF-targeted microbubbles were successfully tested for noninvasive monitoring of tumor angiogenesis in HCC by US.[43,44] Quantitative three-dimensional (3D) DCE-US is also feasible to detect angiogenesis in liver tumor models.[45] A comparison study of contrast-enhanced US (CEUS) and DCE-MRI was performed in a rat model of HCC, and the result showed that DCE-MRI is more accurate than CEUS to evaluate the sorafenib-induced reduction in vascular permeability.[46]

LOW pHe

Molecular imaging techniques are developed for monitoring low pHe, which is largely related to tumor growth, invasion, metastasis, and chemoresistance.[47-50] For example, Pd nanosheet-based radiotracers, ^{131}I-Pd-PEG and ^{125}I-Pd-PEG, were developed for SPECT/CT imaging of HCC.[47] The results showed that the tumor retention of the radiotracer correlates well with the acidic microenvironment. MRI has been used for monitoring pHe in HCC with success in preclinical studies.[48-50] Biosensor imaging of redundant deviation in shifts–based pHe mapping can serve not only as a longitudinal monitoring tool for noninvasive imaging of pHe but also as a functional surrogate biomarker for metabolic changes induced by cTACE of HCC[48,49] (Fig. 2). The pHe mapping of HCC was also achieved by using chemical exchange saturation transfer MRI.[50] In terms of OI, a new near-infrared (NIR) fluorescence probe, DiIRB-S, was developed for monitoring pHe in HCC.[51] The results showed that the probe can target the primary tumors with a high tumor-to-background signal ratio, and a good correlation can
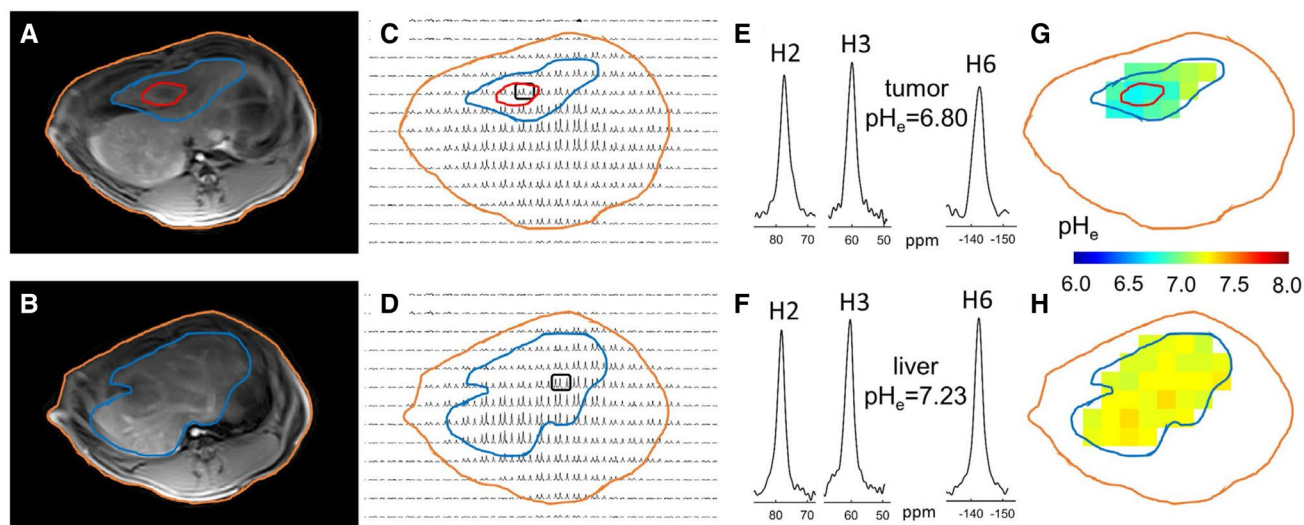
FIG. 2. *In vivo* pHe mapping using biosensor imaging of redundant deviation in shifts with TmDOTP5- in a rabbit liver at 3 T. T_1 VIBE MR images (A,B) were used to localize the VX2 tumor (red contour) within the liver (blue contour), while the profile of the rabbit body is shown with an orange contour. Two different chemical shift imaging (CSI) slices from the same animal were used to show the H2, H3, and H6 MR signals of TmDOTP5- in each voxel, in a part of the liver containing the VX2 tumor (C) and in a part of the liver devoid of any tumor (D). ^{1}H spectra containing the H2, H3, and H6 resonances from the tumor (E) and normal liver (F) indicate a high signal-to-noise ratio in these voxels (>10), allowing accurate pHe determination (6.80 for the tumor and 7.23 for the normal liver). The pHe maps corresponding to the two CSI slices shown in (C) for the liver region with a VX2 tumor and in (D) for a normal liver region are shown in (G) and (H), respectively. The measurements indicate lower average pHe values inside the tumor (6.77 ± 0.03) and in the immediate vicinity of the tumor (6.89 ± 0.09), compared with those for the normal liver (7.22 ± 0.04). Reprinted with permission from Coman et al. (2019). © 2019 Wiley.

be established between the metastatic potential and acidosis distribution pattern in the tumor.

GLYCOLYSIS AND LACTATE

Glycolysis is related to metabolic reprogramming caused by hypoxia in the TME, leading to the over-production of pyruvate, lactate, and carbonic acids. Tumor glycolysis can typically be evaluated using ^{18}F-fluorodeoxyglucose (^{18}F-FDG) PET.[22,52,53] Based on PET/CT imaging, several metabolic parameters, including maximum and mean standardized uptake values, peak standardized uptake values, metabolic tumor volume, and total lesion glycolysis, can be calculated to evaluate glycolysis after IAT of HCC.[22,54] Recently, ^{13}C magnetic resonance spectroscopic imaging (^{13}C-MRSI) of hyperpolarized [1-^{13}C]pyruvate and its metabolites was developed to study energy metabolism by visualizing.[53,55] One study that compared spectroscopic images with ^{18}F-FDG PET for visualizing tumor metabolism in a rat model of HCC revealed that PET and ^{13}C-MRSI

can be used to visualize increased glycolysis flux in HCC malignant tissues.[53] Although the hyperpolarized ^{13}C-MRSI of [1-^{13}C]pyruvate increases the sensitivity of MRI, signal-to-noise ratio constraints still apply for spatially and temporally resolved ^{13}C-MRSI, suggesting the further needs for magnetic resonance (MR) methodologic development (Fig. 3). In addition, an echo-planar 3D ^{13}C-MRSI compression-sensing sequence using hyperpolarized ^{13}C-MRSI was used to rapidly assess and locate the production of lactic acid in precursors, such as ^{13}C-labeled pyruvate or glucose, for imaging of HCC in a preclinical study.[55] Tumor voxels exhibited dramatically elevated lactate/pyruvate ratios (Fig. 4). Although ^{13}C-MRSI is very sensitive for imaging metabolic events, rapid signal decay has a limitation of its broad application.

IFP

Tumor IFP is a physiological parameter that has a predictive value for tumor aggressiveness, drug delivery, as well as response to treatment, such as radiotherapy
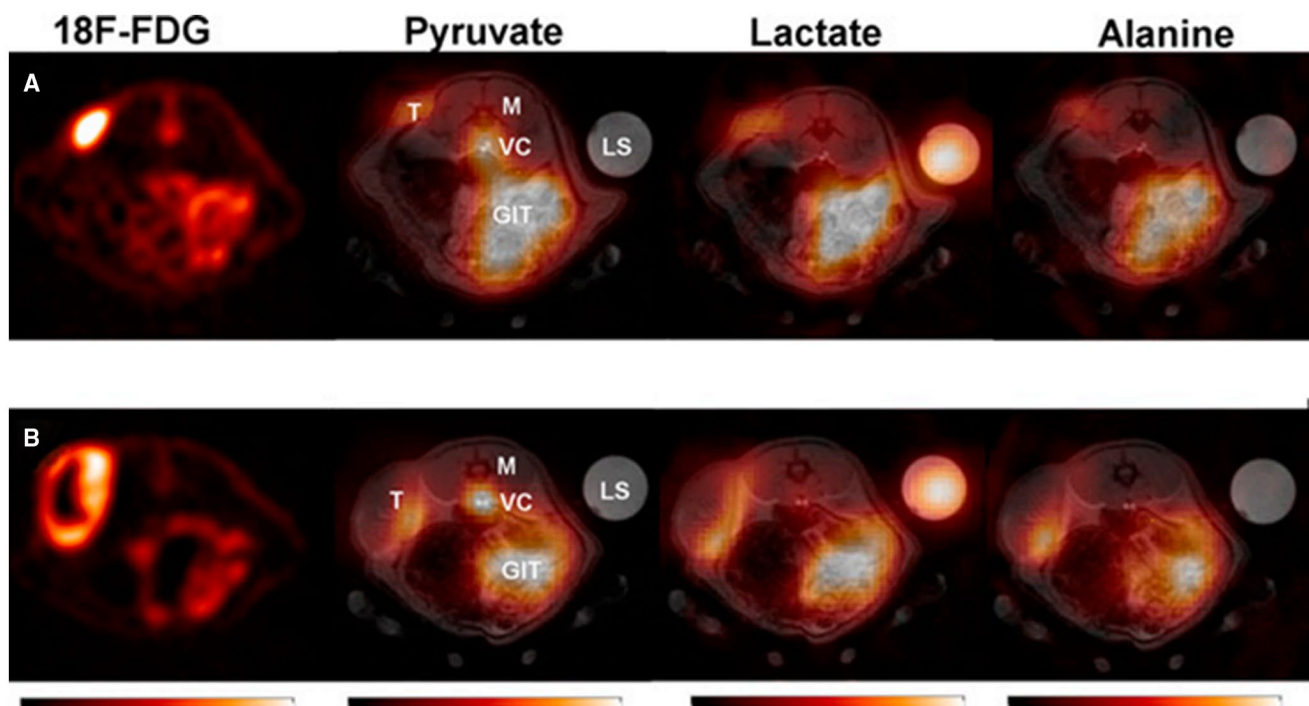
FIG. 3. Examples of ^{13}C MR metabolite images (integrating 30 seconds) and PET images (summing 10 minutes). Color scale was windowed to 6 times background for [1-^{13}C]lactate images and to 10 times background for [1-^{13}C]pyruvate and [1-^{13}C]alanine images. (A) Tumor with high lactate tumor-to-muscle ratio (TMR). (B) Tumor with high lactate TMR despite large necrotic part. Reprinted with permission from Menzel et al. (2013). © 2013 Society of Nuclear Medicine and Molecular Imaging. Abbreviations: GIT, gastrointestinal tract; LS, lactate syringe; M, muscle; T, tumor; and VC, vena cava.

and chemotherapy. Recent studies demonstrated that heterogeneous intratumoral accumulation of liposomes is associated with chaotic tumor microcirculation and elevated IFP. For example, DCE computed tomography (DCE-CT)[56] and DCE-MRI[57] have been used to monitor the IFP of HCC in preclinical studies. Although diffusion-weighted (DW) MRI has been applied for the characterization of the IFP in cervical carcinoma and melanoma,[58,59] the utility of DW-MRI in HCC remains uncertain.

IMMUNE RESPONSE

TME contains a repertoire of immune cells, such as innate tumor-associated macrophages, tumor-associated neutrophils, mast cells, MDSCs, cancer-associated fibroblasts (CAFs), dendritic cells, natural killer cells, Treg cells, and tumor-infiltrating lymphocytes (TILs). It is well-known that immune cell recruitments, various immune responses, and metabolic reprogramming are involved in tumor

development and spread.[17-20] A near-infrared fluorescence probe (IRDye800-AbOX40) was used for noninvasive imaging of OX40 expression on TILs, and it can predict the early response to immunotherapy of HCC.[60] Radiomics has been used as a method to detect the TME of HCC to optimize treatment decisions for immunotherapy. For example, MRI-based immunoscore can be used to evaluate the density of CD3+ and CD8+ T cells,[61] and contrast-enhanced CT-based Rad score was calculated to estimate tumor-infiltrating CD8+ T cells.[62]

CAFs are instrumental in coordinating cellular and molecule in TME, including recombinant extracellular matrix, secreting extracellular matrix metalloproteinases (MMPs), mediating angiogenesis, and regulating the proliferation of tumor and immune cells and migration. The high expression of fibroblast activation protein (FAP) in CAFs has been used as an ideal target for diagnosis. ^{68}Ga-fibroblast activation protein inhibitor (^{68}Ga-FAPI) exhibits excellent target specificity and pharmacokinetics, and it can be used for clinical
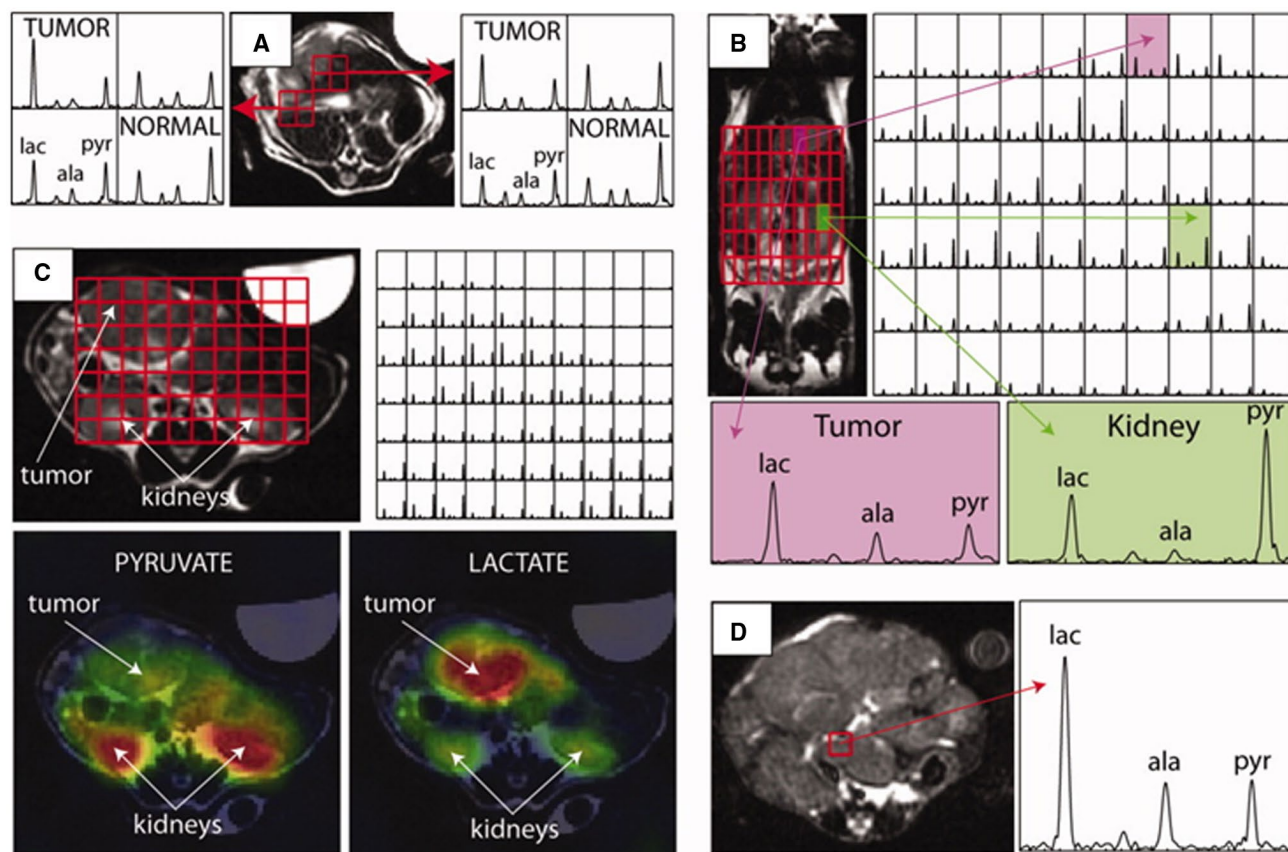
FIG. 4. (A) Spectra from a transgenic liver cancer mouse with an early-stage tumor, as shown in the upper left of the anatomic image, in which acceleration was used to reduce voxel size by a factor of 4 (×3.37 acceleration, 0.034-cm^3 voxel size, 16-second acquisition). Tumor voxels exhibited dramatically elevated lactate/pyruvate ratios. The higher resolution reduced partial volume such that distinct metabolic profiles were observed in tumor and adjacent tissue voxels. (B) A separate data set in the same mouse with the same acquisition parameters in which the 3D-MRSI data are presented coronally to emphasize the distinct metabolic profiles in tumors and other tissues. (C) A 3D-MRSI data set from a different mouse with a moderate-stage tumor at the level of the kidneys. Distinct differences between tumor and normal tissue are readily visualized in the color overlay maps. (D) Data from a mouse with a large very late-stage tumor. Elevated alanine, as well as lactate, was detected in the tumor mass. Reprinted with permission from Hu et al. (2010). © 2009 Wiley.

noninvasive monitoring of CAFs by PET/CT imaging. Increasing evidence shows that ^{68}Ga-FAPI PET/CT imaging is useful for clinical noninvasive detection of CAFs in the TME of HCC.[63,64] ^{68}Ga-FAPI PET/CT should also be considered complementary for tumor entities known to perform poorly with ^{18}F-FDG in HCC. MMPs are proteolytic enzymes that play a key role in the initiation and progression of tumors, and they are related to tumor invasion and metastasis. A dual-modality imaging nanoprobe (Gd-Au@IR820) formed by self-assembly of ultrasmall AuNPs modified with MMP-2 on the surface was used for dual-mode (MRI/FLI) real-time imaging-guided photodynamic/photothermal combination

therapy for HCC.[65] In another study, NIR dye-labeled MMP was used as a molecular probe to successfully detect MMP of HCC using FLI.[66] RGD, MMP, and ^{18}F-FDG were imaged on tumor-bearing mice using PET, CT, X-ray, and multi-wavelength OI modalities.[66] Image results revealed that each agent is bound to a specific disease target component.

OTHER MOLECULAR TARGETS

TACE with immunotherapies can exploit tumor-associated antigens that are exposed during tissue destruction and presented by antigen-presenting immune cells (APCs) to activate T-lymphocytes.[67]

A study demonstrated that specific gadolinium 160-labeled anti-human leukocyte antigen–DR isotope antibodies (160Gd-HLA-DR antibodies) and superparamagnetic iron oxide nanoparticles (SPIONs) showed curvilinear peritumoral distribution on MRI scans in a VX2 rabbit liver tumor model, corresponding to APCs and iron deposits in macrophages, respectively.[68] In addition, glypican-3 (GPC3) is a carcinoembryonic antigen that is an ideal target for anticancer immunotherapy against HCC. A study showed that patients with GPC3-expressing HCCs exhibited an increase in GPC3-specific cytotoxic T lymphocytes after RFA or TACE, whereas none of the patients did after surgical resection.[69] Molecular probes for targeting GPC3 are actively being developed for PET and OI.[70-73]

Conclusion and Perspectives

Cancer immunotherapy has undergone a rapid expansion in terms of the number of agents that confer a prognostic benefit by activating the immune system to mount a response against developing tumors. Recently, immunotherapy approaches that involve blocking the immune-suppressive cytotoxic T-lymphocyte-associated protein 4 or programmed cell death protein 1 have shown promising results.[74] However, the distinction between hot, altered, and cold tumors relies on the cytotoxic T-cell landscape within a tumor. Monitoring of TME with thorough profiling can better analyze the complexity of the tumors and provide dynamic information about the complex network changes occurring in the TME to assist in clinical decisions.[75] With the advent of immunotherapy for HCC, there is an increasing interest in understanding how immunotherapy may be best combined with locoregional therapies.[9,76] Currently, a good number of phase 2 and 3 clinical trials are investigating the combined locoregional-immunotherapy,[4,9] such as the combination of TACE and immunotherapy (NCT04268888, NCT04246177, NCT03778957, NCT03575806, NCT03572582, NCT03592706, NCT03397654, NCT02856815, NCT02568748, and NCT02487017); the combination of ablation and immunotherapy (NCT03383458); the combination of TACE, ablation, and immunotherapy (NCT03124498 and NCT02821754); and the combination of Y90 and immunotherapy (NCT02837029, NCT03380130,

NCT03033446, and NCT03099564). As new treatment approaches are being developed, noninvasive assessment, in real time, of tumor response to treatment currently remains a major challenge. Imaging tools to assist in this clinical decision-making process, thus enabling treatment optimization for the individual patient, are therefore urgently needed.

Clinically, assessment of response to LRT includes the measurement of tumor size, tumor margins, tumor necrosis, and the detection of residual or recurring and new tumors. Advances in morphological imaging techniques, particularly MRI and CT, have improved the detection and staging of tumors, as well as the measurement of therapy response.[77,78] Further improvement in the HCC patient management through imaging will be limited unless anatomical studies are augmented with an assessment of tumor biology and metabolism *in vivo*. Metabolic imaging can be an excellent supplementary method for evaluating the response of LRT in HCC. PET and SPECT imaging modalities have been used to monitor the response of locoregional therapy in HCC.[77-79] Recently, a clinical trial showed that ^{18}F-fluorocholine (^{18}F-FCH) PET/CT can predict the outcome of early-stage HCC undergoing LRT.[80] Compared with FDG, ^{18}F-FCH is considered to be more sensitive in detecting HCC, especially for well-differentiated HCC.[81]

Image-guided surgery can visually distinguish tumor cells from surrounding tissues in real time, thereby facilitating the complete removal of tumor lesions.[82,83] Indocyanine green (ICG) is the most popular imaging agent used for image-guided surgery, and it has been approved by the U.S. Food and Drug Administration for surgical procedures.[84,85] In addition to ICG, many fluorescent dyes, including Cy5.5, Cy7, IRdye800 CW, and quantum dots have been extensively studied.[83] After the conjugation with tumor-specific ligands of biomarkers, such as matrix metalloproteinase and integrin $\alpha_v\beta_3$, the imaging probes can enhance intraoperative tumor-specific uptake.[82] It is expected that imaging tools will continue to play an important role in the LRT of HCC, including surgical resection.

Due to the heterogeneity of HCC and the complexity of the TME, combinations of imaging techniques, as so-called "multimodality imaging," are being designed to take the strengths of modalities while minimizing their limitations, which as a result may simultaneously provide comprehensive biological

information. Although recent preclinical data are quite promising in the assessment of treatment response in HCC, a huge effort remains required to accelerate the translation of new imaging techniques from bench to bedside. To foster the continued discovery and development of imaging techniques, strong collaborations among academia, industry, and government are pivotal. In the foreseeable future, it is expected that molecular imaging techniques will be extensively applied in clinical settings and thus pave the way toward personalized cancer medicine to improve the management of patients with HCC.

REFERENCES

1) Sung H, Ferlay J, Siegel RL, Laversanne M, Soerjomataram I, Jemal A, et al. Global cancer statistics 2020: GLOBOCAN estimates of incidence and mortality worldwide for 36 cancers in 185 countries. CA Cancer J Clin 2021;71:209-249.

2) Akinyemiju T, Abera S, Ahmed M, Alam N, Alemayohu MA, Allen C, et al. The burden of primary liver cancer and underlying etiologies from 1990 to 2015 at the global, regional, and national level: results from the global burden of disease study 2015. JAMA Oncol 2017;3:1683-1691.

3) Makary MS, Khandpur U, Cloyd JM, Mumtaz K, Dowell JD. Locoregional therapy approaches for hepatocellular carcinoma: recent advances and management strategies. Cancers (Basel) 2020;12:1914.

4) Kloeckner R, Galle PR, Bruix J. Local and regional therapies for hepatocellular carcinoma. Hepatology 2021;73(Suppl 1):137-149.

5) Lencioni R. Loco-regional treatment of hepatocellular carcinoma. Hepatology 2010;52:762-773.

6) Liu J, Dang H, Wang XW. The significance of intertumor and intratumor heterogeneity in liver cancer. Exp Mol Med 2018;50:e416.

7) Liu K, Zhang X, Xu W, Chen J, Yu J, Gamble JR, et al. Targeting the vasculature in hepatocellular carcinoma treatment: Starving versus normalizing blood supply. Clin Transl Gastroenterol 2017;8:e98.

8) Walsh JC, Lebedev A, Aten E, Madsen K, Marciano L, Kolb HC. The clinical importance of assessing tumor hypoxia: relationship of tumor hypoxia to prognosis and therapeutic opportunities. Antioxid Redox Signal 2014;21:1516-1554.

9) Greten TF, Mauda-Havakuk M, Heinrich B, Korangy F, Wood BJ. Combined locoregional-immunotherapy for liver cancer. J Hepatol 2019;70:999-1007.

10) Tong Y, Yang H, Xu X, Ruan J, Liang M, Wu J, et al. Effect of a hypoxic microenvironment after radiofrequency ablation on residual hepatocellular cell migration and invasion. Cancer Sci 2017;108:753-762.

11) **Zhou C**, **Yao QI**, Zhang H, Guo X, Liu J, Shi Q, et al. Combining transcatheter arterial embolization with iodized oil containing Apatinib inhibits HCC growth and metastasis. Sci Rep 2020;10:2964.

12) Li W, Quan YY, Li Y, Lu L, Cui M. Monitoring of tumor vascular normalization: the key points from basic research to clinical application. Cancer Manag Res 2018;10:4163-4172.

13) Weber WA, Czernin J, Anderson CJ, Badawi RD, Barthel H, Bengel F, et al. The future of nuclear medicine, molecular imaging, and theranostics. J Nucl Med 2020;61:263S-272S.

14) Bouche M, Hsu JC, Dong YC, Kim J, Taing K, Cormode DP. Recent advances in molecular imaging with gold nanoparticles. Bioconjug Chem 2020;31:303-314.

15) Chen K, Chen X. Positron emission tomography imaging of cancer biology: current status and future prospects. Semin Oncol 2011;38:70-86.

16) Ibrahim AA, Schmithals C, Kowarz E, Koberle V, Kakoschky B, Pleli T, et al. Hypoxia causes downregulation of dicer in hepatocellular carcinoma, which Is required for upregulation of hypoxia-inducible factor 1 alpha and epithelial-mesenchymal transition. Clin Cancer Res 2017;23:3896-3905.

17) Ramamonjisoa N, Ackerstaff E. Characterization of the tumor microenvironment and tumor-stroma interaction by non-invasive preclinical imaging. Front Oncol 2017;7:3.

18) **Yang JD**, **Nakamura I**, Roberts LR. The tumor microenvironment in hepatocellular carcinoma: current status and therapeutic targets. Semin Cancer Biol 2011;21:35-43.

19) **Hernandez-Gea V**, **Toffanin S**, Friedman SL, Llovet JM. Role of the microenvironment in the pathogenesis and treatment of hepatocellular carcinoma. Gastroenterology 2013;144:512-527.

20) Giannelli G, Rani B, Dituri F, Cao Y, Palasciano G. Moving towards personalised therapy in patients with hepatocellular carcinoma: the role of the microenvironment. Gut 2014;63:1668-1676.

21) **Zhou D-Y**, **Qin J**, Huang J, Wang F, Xu G-P, Lv Y-T, et al. Zoledronic acid inhibits infiltration of tumor-associated macrophages and angiogenesis following transcatheter arterial chemoembolization in rat hepatocellular carcinoma models. Oncol Lett 2017;14:4078-4084.

22) Schobert I, Chapiro J, Pucar D, Saperstein L, Savic LJ. Fluorodeoxyglucose PET for monitoring response to embolotherapy (transarterial chemoembolization) in primary and metastatic liver tumors. PET Clin 2019;14:437-445.

23) Chang X, Lu X, Guo J, Teng GJ. Interventional therapy combined with immune checkpoint inhibitors: emerging opportunities for cancer treatment in the era of immunotherapy. Cancer Treat Rev 2019;74:49-60.

24) Riedl CC, Brader P, Zanzonico P, Reid V, Woo Y, Wen B, et al. Tumor hypoxia imaging in orthotopic liver tumors and peritoneal metastasis: a comparative study featuring dynamic ^{18}F-MISO and ^{124}I-IAZG PET in the same study cohort. Eur J Nucl Med Mol Imaging 2008;35:39-46.

25) Riedl CC, Brader P, Zanzonico PB, Chun YS, Woo Y, Singh P, et al. Imaging hypoxia in orthotopic rat liver tumors with iodine 124-labeled iodoazomycin galactopyranoside PET. Radiology 2008;248:561-570.

26) Evans SM, Kachur AV, Shiue CY, Hustinx R, Jenkins WT, Shive GG, et al. Noninvasive detection of tumor hypoxia using the 2-nitroimidazole [^{18}F]EF1. J Nucl Med 2000;41:327-336.

27) Ziemer L, Evans S, Kachur A, Shuman A, Cardi C, Jenkins W, et al. Noninvasive imaging of tumor hypoxia in rats using the 2-nitroimidazole ^{18}F-EF5. Eur J Nucl Med Mol Imaging 2003;30:259-266.

28) Bane O, Besa C, Wagner M, Oesingmann N, Zhu H, Fiel MI, et al. Feasibility and reproducibility of BOLD and TOLD measurements in the liver with oxygen and carbogen gas challenge in healthy volunteers and patients with hepatocellular carcinoma. J Magn Reson Imaging 2016;43:866-876.

29) Patterson AJ, Priest AN, Bowden DJ, Wallace TE, Patterson I, Graves MJ, et al. Quantitative BOLD imaging at 3T: temporal changes in hepatocellular carcinoma and fibrosis following oxygen challenge. J Magn Reson Imaging 2016;44:739-744.

30) Huang Z, Xu X, Meng X, Hou Z, Liu F, Hua Q, et al. Correlations between ADC values and molecular markers of

Ki-67 and HIF-1alpha in hepatocellular carcinoma. Eur J Radiol 2015;84:2464-2469.

31) Yopp AC, Schwartz LH, Kemeny N, Gultekin DH, Gönen M, Bamboat Z, et al. Antiangiogenic therapy for primary liver cancer: correlation of changes in dynamic contrast-enhanced magnetic resonance imaging with tissue hypoxia markers and clinical response. Ann Surg Oncol 2011;18:2192-2199.

32) Zhang L, Shan X, Guo L, Zhang J, Ge J, Jiang Q, et al. A sensitive and fast responsive fluorescent probe for imaging hypoxic tumors. Analyst 2018;144:284-289.

33) Lee S, Kim JH, Lee JH, Lee JH, Han JK. Non-invasive monitoring of the therapeutic response in sorafenib-treated hepatocellular carcinoma based on photoacoustic imaging. Eur Radiol 2018;28: 372-381.

34) Jin Z-H, Furukawa T, Claron M, Boturyn D, Coll J-L, Fukumura T, et al. Positron emission tomography imaging of tumor angiogenesis and monitoring of antiangiogenic efficacy using the novel tetrameric peptide probe ^{64}Cu-cyclam-RAFT-c(-RGDfK-)4. Angiogenesis 2012;15:569-580.

35) Zheng J, Miao W, Huang C, Lin H. Evaluation of ^{99m}Tc-3PRGD2 integrin receptor imaging in hepatocellular carcinoma tumour-bearing mice: comparison with ^{18}F-FDG metabolic imaging. Ann Nucl Med 2017;31:486-494.

36) Ma W, Kang F, Wang Z, Yang W, Li G, Ma X, et al. ^{99m}Tc-labeled monomeric and dimeric NGR peptides for SPECT imaging of CD13 receptor in tumor-bearing mice. Amino Acids 2013;44: 1337-1345.

37) Barrett T, Brechbiel M, Bernardo M, Choyke PL. MRI of tumor angiogenesis. J Magn Reson Imaging 2007;26:235-249.

38) Qian T, Chen M, Gao F, Meng F, Gao X, Yin H. Diffusion-weighted magnetic resonance imaging to evaluate microvascular density after transarterial embolization ablation in a rabbit VX2 liver tumor model. Magn Reson Imaging 2014;32:1052-1057.

39) Choi J-I, Imagawa DK, Bhosale P, Bhargava P, Tirkes T, Seery TE, et al. Magnetic resonance imaging following treatment of advanced hepatocellular carcinoma with sorafenib. Clin Mol Hepatol 2014;20:218-222.

40) **Chen J, Qian T**, Zhang H, Wei C, Meng F, Yin H. Combining dynamic contrast enhanced magnetic resonance imaging and microvessel density to assess the angiogenesis after PEI in a rabbit VX2 liver tumor model. Magn Reson Imaging 2016;34: 177-182.

41) **Jia Z, Song L**, Zang F, Song J, Zhang W, Yan C, et al. Active-target T1-weighted MR imaging of tiny hepatic tumor via RGD modified ultra-small Fe_3O_4 nanoprobes. Theranostics 2016;6: 1780-1791.

42) Chen J, White SB, Harris KR, Li W, Yap JWT, Kim D-H, et al. Poly(lactide-co-glycolide) microspheres for MRI-monitored delivery of sorafenib in a rabbit VX2 model. Biomaterials 2015;61: 299-306.

43) Yuan HX, Wang WP, Wen JX, Lin LW, Exner AA, Guan PS, et al. Dual-targeted microbubbles specific to integrin alphaVbeta3 and vascular endothelial growth factor receptor 2 for ultrasonography evaluation of tumor angiogenesis. Ultrasound Med Biol 2018;44:1460-1467.

44) Wang L, Lu YH, Wang TY. Value of ultrasound-targeted vascular endothelial growth factor receptor-2 in non-invasive monitoring of anti-angiogenic response in nude mice with subcutaneous xenograft model. Zhonghua Zhong Liu Za Zhi 2020;42:856-860.

45) **Zheng Q, Zhang J-C**, Wang Z, Ruan S-M, Li W, Pan F-S, et al. Assessment of angiogenesis in rabbit orthotropic liver tumors using three-dimensional dynamic contrast-enhanced ultrasound compared with two-dimensional DCE-US. Jpn J Radiol 2019;37:701-709.

46) Muñoz NM, Minhaj AA, Maldonado KL, Kingsley CV, Cortes AC, Taghavi H, et al. Comparison of dynamic contrast-enhanced magnetic resonance imaging and contrast-enhanced ultrasound for evaluation of the effects of sorafenib in a rat model of hepatocellular carcinoma. Magn Reson Imaging 2019;57:156-164.

47) **Chen M, Guo Z**, Chen Q, Wei J, Li J, Shi C, et al. Pd nanosheets with their surface coordinated by radioactive iodide as a high-performance theranostic nanoagent for orthotopic hepatocellular carcinoma imaging and cancer therapy. Chem Sci 2018;9:4268-4274.

48) Savic LJ, Schobert IT, Peters D, Walsh JJ, Laage-Gaupp FM, Hamm CA, et al. Molecular imaging of extracellular tumor pH to reveal effects of locoregional therapy on liver cancer microenvironment. Clin Cancer Res 2020;26:428-438.

49) Coman D, Peters DC, Walsh JJ, Savic LJ, Huber S, Sinusas AJ, et al. Extracellular pH mapping of liver cancer on a clinical 3T MRI scanner. Magn Reson Med 2020;83:1553-1564.

50) **Chen M, Chen C**, Shen Z, Zhang X, Chen Y, Lin F, et al. Extracellular pH is a biomarker enabling detection of breast cancer and liver cancer using CEST MRI. Oncotarget 2017;8:45759-45767.

51) Wang L, Fan Z, Zhang J, Changyi Y, Huang C, Gu Y, et al. Evaluating tumor metastatic potential by imaging intratumoral acidosis via pH-activatable near-infrared fluorescent probe. Int J Cancer 2015;136:E107-E116.

52) Zhang LF, Lou JT, Lu MH, Gao C, Zhao S, Li B, et al. Suppression of miR-199a maturation by HuR is crucial for hypoxia-induced glycolytic switch in hepatocellular carcinoma. EMBO J 2015;34:2671-2685.

53) Menzel MI, Farrell EV, Janich MA, Khegai O, Wiesinger F, Nekolla S, et al. Multimodal assessment of *in vivo* metabolism with hyperpolarized [1-^{13}C]MR spectroscopy and ^{18}F-FDG PET imaging in hepatocellular carcinoma tumor-bearing rats. J Nucl Med 2013;54:1113-1119.

54) Sager S, Akgün E, Uslu-Beşli L, Asa S, Akovali B, Sahin O, et al. Comparison of PERCIST and RECIST criteria for evaluation of therapy response after yttrium-90 microsphere therapy in patients with hepatocellular carcinoma and those with metastatic colorectal carcinoma. Nucl Med Commun 2019;40:461-468.

55) Hu S, Lustig M, Balakrishnan A, Larson PE, Bok R, Kurhanewicz J, et al. 3D compressed sensing for highly accelerated hyperpolarized ^{13}C MRSI with *in vivo* applications to transgenic mouse models of cancer. Magn Reson Med 2010;63:312-321.

56) Stapleton S, Milosevic M, Allen C, Zheng J, Dunne M, Yeung I, et al. A mathematical model of the enhanced permeability and retention effect for liposome transport in solid tumors. PLoS One 2013;8:e81157.

57) Liu LJ, Brown SL, Ewing JR, Ala BD, Schneider KM, Schlesinger M. Estimation of tumor interstitial fluid pressure (TIFP) noninvasively. PLoS One 2016;11:e0140892.

58) Hompland T, Ellingsen C, Galappathi K, Rofstad EK. Connective tissue of cervical carcinoma xenografts: associations with tumor hypoxia and interstitial fluid pressure and its assessment by DCE-MRI and DW-MRI. Acta Oncol 2014;53:6-15.

59) Hompland T, Ellingsen C, Galappathi K, Rofstad EK. DW-MRI in assessment of the hypoxic fraction, interstitial fluid pressure, and metastatic propensity of melanoma xenografts. BMC Cancer 2014;14:92.

60) Chen X, Li D, Cao Y, Gao J, Jin H, Shan H. Early therapeutic vaccination prediction of hepatocellular carcinoma via imaging OX40-mediated tumor infiltrating lymphocytes. Mol Pharm 2019;16:4252-4259.

61) **Chen S, Feng S**, Wei J, Liu F, Li B, Li X, et al. Pretreatment prediction of immunoscore in hepatocellular cancer: a radiomics-based clinical model based on Gd-EOB-DTPA-enhanced MRI imaging. Eur Radiol 2019;29:4177-4187.

62) **Liao H, Zhang Z**, Chen J, Liao M, Xu L, Wu Z, et al. Preoperative radiomic approach to evaluate tumor-infiltrating CD8+ T cells in

hepatocellular carcinoma patients using contrast-enhanced computed tomography. Ann Surg Oncol 2019;26:4537-4547.

63) **Giesel FL, Kratochwil C**, Lindner T, Marschalek MM, Loktev A, Lehnert W, et al. ^{68}Ga-FAPI PET/CT: biodistribution and preliminary dosimetry estimate of 2 DOTA-containing FAP-targeting agents in patients with various cancers. J Nucl Med 2019;60:386-392.

64) **Chen H, Pang Y, Wu J**, Zhao L, Hao B, Wu J, et al. Comparison of [^{68}Ga]Ga-DOTA-FAPI-04 and [^{18}F]FDG PET/CT for the diagnosis of primary and metastatic lesions in patients with various types of cancer. Eur J Nucl Med Mol Imaging 2020;47:1820-1832.

65) **Li B, Sun L**, Li T, Zhang Y, Niu X, Xie M, et al. Ultra-small gold nanoparticles self-assembled by gadolinium ions for enhanced photothermal/photodynamic liver cancer therapy. J Mater Chem B 2021;9:1138-1150.

66) **Ke S, Zhang F, Wang W**, Qiu X, Lin J, Cameron AG, et al. Multiple target-specific molecular imaging agents detect liver cancer in a preclinical model. Curr Mol Med 2012;12:944-951.

67) Mizukoshi E, Yamashita T, Arai K, Sunagozaka H, Ueda T, Arihara F, et al. Enhancement of tumor-associated antigen-specific T cell responses by radiofrequency ablation of hepatocellular carcinoma. Hepatology 2013;57:1448-1457.

68) Savic LJ, Doemel LA, Schobert IT, Montgomery RR, Joshi N, Walsh JJ, et al. Molecular MRI of the immuno-metabolic interplay in a rabbit liver tumor model: a biomarker for resistance mechanisms in tumor-targeted therapy? Radiology 2020;296:575-583.

69) Nobuoka D, Motomura Y, Shirakawa H, Yoshikawa T, Kuronuma T, Takahashi M, et al. Radiofrequency ablation for hepatocellular carcinoma induces glypican-3 peptide-specific cytotoxic T lymphocytes. Int J Oncol 2012;40:63-70.

70) **Li Y, Zhang J**, Gu J, Hu K, Huang S, Conti PS, et al. Radiofluorinated GPC3-binding peptides for PET imaging of hepatocellular carcinoma. Mol Imaging Biol 2020;22:134-143.

71) Mu W, Jiang D, Mu S, Liang S, Liu Y, Zhang N. Promoting early diagnosis and precise therapy of hepatocellular carcinoma by glypican-3-targeted synergistic chemo-photothermal theranostics. ACS Appl Mater Interfaces 2019;11:23591-23604.

72) Qin Z, Wang J, Wang YE, Wang G, Wang X, Zhou Z, et al. Identification of a glypican-3-binding peptide for *in vivo* non-invasive human hepatocellular carcinoma detection. Macromol Biosci 2017;17:1600335.

73) Sham JG, Kievit FM, Grierson JR, Miyaoka RS, Yeh MM, Zhang M, et al. Glypican-3-targeted [89]Zr PET imaging of hepatocellular carcinoma. J Nucl Med 2014;55:799-804.

74) Benavente S, Sanchez-Garcia A, Naches S, LLeonart ME, Lorente J. Therapy-induced modulation of the tumor microenvironment: new opportunities for cancer therapies. Front Oncol 2020;10:582884.

75) Petitprez F, Meylan M, de Reynies A, Sautes-Fridman C, Fridman WH. The tumor microenvironment in the response to immune checkpoint blockade therapies. Front Immunol 2020;11:784.

76) Singh P, Toom S, Avula A, Kumar V, Rahma OE. The immune modulation effect of locoregional therapies and its potential synergy with immunotherapy in hepatocellular carcinoma. J Hepatocell Carcinoma 2020;7:11-17.

77) Yaghmai V, Besa C, Kim E, Gatlin JL, Siddiqui NA, Taouli B. Imaging assessment of hepatocellular carcinoma response to locoregional and systemic therapy. AJR Am J Roentgenol 2013;201:80-96.

78) Gonzalez-Guindalini FD, Botelho MPF, Harmath CB, Sandrasegaran K, Miller FH, Salem R, et al. Assessment of liver tumor response to therapy: role of quantitative imaging. Radiographics 2013;33:1781-1800.

79) Dierckx R, Maes A, Peeters M, Van De Wiele C. FDG PET for monitoring response to local and locoregional therapy in HCC and liver metastases. Q J Nucl Med Mol Imaging 2009;53: 336-342.

80) Wallace MC, Sek K, Francis RJ, Samuelson S, Ferguson J, Tibballs J, et al. Baseline and post-treatment ^{18}F-Fluorocholine PET/CT predicts outcomes in hepatocellular carcinoma following locoregional therapy. Dig Dis Sci 2020;65:647-657.

81) Talbot J-N, Gutman F, Fartoux L, Grange J-D, Ganne N, Kerrou K, et al. PET/CT in patients with hepatocellular carcinoma using [^{18}F]fluorocholine: preliminary comparison with [^{18}F]FDG PET/CT. Eur J Nucl Med Mol Imaging 2006;33:1285-1289.

82) Wang C, Wang Z, Zhao T, Li Y, Huang G, Sumer BD, et al. Optical molecular imaging for tumor detection and image-guided surgery. Biomaterials 2018;157:62-75.

83) Chi C, Du Y, Ye J, Kou D, Qiu J, Wang J, et al. Intraoperative imaging-guided cancer surgery: from current fluorescence molecular imaging methods to future multi-modality imaging technology. Theranostics 2014;4:1072-1084.

84) Golriz M, Majlesara A, El Sakka S, Ashrafi M, Arwin J, Fard N, et al. Small for size and flow (SFSF) syndrome: an alternative description for posthepatectomy liver failure. Clin Res Hepatol Gastroenterol 2016;40:267-275.

85) Fan Z, Zong J, Lau WY, Zhang Y. Indocyanine green and its nanosynthetic particles for the diagnosis and treatment of hepatocellular carcinoma. Am J Transl Res 2020;12:2344-2352.

86) Wang Y, Stewart E, Desjardins L, Hadway J, Morrison L, Crukley C, et al. Assessment of intratumor hypoxia by integrated ^{18}F-FDG PET/perfusion CT in a liver tumor model. PLoS One 2017;12:e0173016.

87) Stapleton S, Milosevic M, Tannock IF, Allen C, Jaffray DA. The intra-tumoral relationship between microcirculation, interstitial fluid pressure and liposome accumulation. J Control Release 2015;211:163-170.

Author names in bold designate shared co-first authorship.